



Extratropical forcing of ENSO

Ghyslaine Boschat, Pascal Terray, Sébastien Masson

► To cite this version:

Ghyslaine Boschat, Pascal Terray, Sébastien Masson. Extratropical forcing of ENSO. *Geophysical Research Letters*, 2013, 40, pp.1605-1611. 10.1002/GRL.50229 . hal-00873386

HAL Id: hal-00873386

<https://hal.science/hal-00873386>

Submitted on 30 May 2016

HAL is a multi-disciplinary open access archive for the deposit and dissemination of scientific research documents, whether they are published or not. The documents may come from teaching and research institutions in France or abroad, or from public or private research centers.

L'archive ouverte pluridisciplinaire **HAL**, est destinée au dépôt et à la diffusion de documents scientifiques de niveau recherche, publiés ou non, émanant des établissements d'enseignement et de recherche français ou étrangers, des laboratoires publics ou privés.

1
2 **Extratropical forcing of ENSO**
3
4

5 Ghyslaine Bosch¹, Pascal Terray², Sébastien Masson³
6

7 *LOCEAN/IPSL, CNRS/IRD/UPMC/MNHN, Paris, France*
8
9
10
11
12
13

14 To be submitted to *Geophysical Research Letters*
15

16 February 2013
17
18
19
20

¹ Corresponding author: Ghyslaine Bosch, LOCEAN-IPSL,
Université Pierre et Marie Curie, BP100 – 4 place Jussieu, 75252 Paris cedex 05, France.
Tel : +33 1 44 27 23 29
E-mail : gbolod@locean-ipsl.upmc.fr

² Pascal TERRAY, LOCEAN-IPSL, UMR 7617 CNRS/IRD/UPMC/MNHN
Université Pierre et Marie Curie, BP 100 - 4 Place Jussieu 75252 Paris cedex 05 France
Tel : +33 1 44 27 70 78
E-mail : pascal.terray@locean-ipsl.upmc.fr

³ Sébastien MASSON, LOCEAN-IPSL,
Université Pierre et Marie Curie, BP100 – 4 place Jussieu, 75252 Paris cedex 05, France.
Tel : +33 1 44 27 27 48
E-mail : sebastien.masson@locean-ipsl.upmc.fr

1. Abstract

We present evidence that Sea Surface Temperatures (SSTs) in the North Pacific, South Atlantic and Indian Oceans (AO and IO, respectively) during late boreal winter, offer another important source of predictability for El Niño Southern Oscillation (ENSO). This new SST predictor may provide accurate prediction of the *amplitude* of ENSO events before their onset, for both El Niño and La Niña events which occurred during recent decades.

2. Introduction

According to many studies, the crucial set of information for ENSO forecasts lies in the spatial variation of the thermocline depth or heat content (Meinen and McPhaden, 2000; McPhaden 2003) and the low-frequency wind variability in the tropical Indo-Pacific region (Clarke and Van Gorder, 2003). An influence from high-frequency wind variability in the western Pacific region has also been suggested, but so far the most robust leading relationship has been observed with the Madden Julian Oscillation activity in late boreal spring or early summer, therefore after the ENSO onset period (Hendon et al., 2007).

Nevertheless, there has been growing evidence in the literature, that other tropical and extratropical regions may also be playing an important role for ENSO. First, a number of studies suggested a close link with SST anomalies in the tropical IO or AO, which may induce modulations of the Walker circulations (Kug et al., 2005; Dommenget et al., 2006; Rodriguez-Fonseca et al., 2009; Izumo et al., 2010; Frauen and Dommenget, 2012). Recently, there has also been a rising interest in the predictability offered by *extratropical* climate modes of variability. Vimont et al. (2003) and Wang et al. (2012) have implied a connection between the mid-latitude and tropical Pacific, whereby the winter atmospheric variability in the North Pacific

impacts subtropical SST variability and western Pacific equatorial wind anomalies, which may be responsible for exciting subsequent El Niño events. Several recent studies also emphasized the role of mid-latitude coupled variability in the South AO and IO during late boreal winter (Terray and Dominiak, 2005; Terray, 2011).

However, several open questions remain regarding the *pertinence* or added value of these new ‘extratropical’ precursors for the forecast of ENSO, compared to the conventional Pacific wind or heat content predictors, or the other tropical SST predictors. In this study, we combine the newly proposed sources of ENSO predictability in the North Pacific, South AO and IO, and evaluate the potential efficiency of this new SST predictor in predicting ENSO onset and amplitude across the “spring predictability barrier” (Webster and Yang, 1992). We present evidence, through statistical analyses of observations and a coupled ocean-atmosphere model simulation, that this new SST precursor may offer an important source of predictability for ENSO.

3. Data and Methods

We compare three precursors of ENSO in late boreal winter: the upper-ocean heat content (Z20 precursor) and low-frequency zonal wind stress variability (USTR precursor) in the tropical Pacific, and SST variability in the North Pacific, South AO and IO (new SST precursor). We focus our analysis on the recent period after 1979, since records of tropical Pacific heat content and SST in the South AO and IO are either sparse or inexistent before this date.

The depth of the 20°C isotherm (Z20) is used as a proxy of the thermocline depth or heat content in the tropical Pacific Ocean, and is extracted from the Simple Ocean Data Assimilation (SODA) reanalysis (Carton and Giese, 2008; SODA version 2.2.4), available until 2008. We examine atmospheric fields from the ERA-Interim reanalysis

(Dee et al., 2011) and SST fields from the Hadley Centre Global Sea Ice and Sea Surface Temperature (HadISST1.1) dataset (Rayner et al., 2003), both available until 2011. For each field, monthly anomalies are calculated by applying the Seasonal-Trend decomposition procedure based on Loess (Cleveland et al., 1990), which filters out any long-term trends and annual cycle in the initial data.

Our goal is to predict the ENSO peak phase, which is defined by SST anomalies averaged from October to the following February (ONDJF) over the *entire* equatorial Pacific. The precursors are taken either from January to March (JFM) or February to April (FMA), 9 or 10 months prior to this typical ENSO peak phase. Sensitivity analyses have been performed with the precursors taken successively in JFM, FMA or from March to May (MAM), and for each case, we have chosen the season which offers the best skill for the following ENSO.

In order to compare the Z20, USTR and new SST precursors, we use the Singular Value Decomposition (SVD) method (Bretherton et al., 1992), which we apply separately between each precursor field during its peaking season and the following tropical Pacific SST field during boreal winter. Results are shown for the 1st SVD mode associated with each precursor in terms of the corresponding Expansion Coefficient (EC) time series, the ‘homogeneous’ map for the precursor (i.e regression map between the precursor field and its corresponding EC time series) and ‘heterogeneous’ map for the predicted ENSO field (i.e regression map between the tropical Pacific SST and the EC time series of the precursor field, indicating how well the grid point anomalies of the ENSO field can be predicted from the precursor’s EC time series). The statistics provided by the SVD are also efficient tools for quantifying the relevance of each ENSO precursor. The Squared Covariance Fraction (SCF) measures the relative importance of each SVD mode in reconstructing the covariance

matrix between the precursor field and tropical Pacific SSTs. The correlation coefficient (r) between the EC time series of the two fields indicate how strongly related the coupled patterns are. Finally, we computed how much of Pacific SST variance each SVD mode explains, and the correlations between the SVD modes and the Niño3.4 SST time series during the following winter.

To test the robustness of our results, we also performed similar SVD analyses on a 110-year control simulation of the SINTEX-F2 global coupled ocean-atmosphere general (CGCM) model, since it exhibits a realistic ENSO (Masson et al., 2012).

4. Analysis and Results

4.1 Heat content and zonal wind predictors

We here examine the conventional Z20 and USTR predictors and assess their relationships with the following ENSO event, within our SVD framework (Fig. 1 and Table 1). During the 1979-2008 period, the 1st SVD mode between the Z20 precursor and ENSO is consistent with the predicting potential of heat content in the context of ENSO forecasting (McPhaden, 2003). Indeed, the Z20 pattern in Fig. 1 is marked by positive Z20 anomalies in the west-central tropical Pacific in spring and appears as a mixture of the two leading Empirical Orthogonal Functions (EOFs) of Pacific Z20 variability (see Meinen and McPhaden, 2000); while the corresponding SST pattern (Fig. 1b) illustrates a typical El Niño peak phase during the following winter (consistent with figure 5 in McPhaden, 2003). This SST pattern also suggests that the performance of the Z20 precursor is degraded in the far eastern equatorial Pacific.

The statistics of this 1st SVD mode (shown in Table 1) confirm that Z20 anomalies during late boreal winter are strongly correlated with SST anomalies in the tropical Pacific ($r=0.71$), and that this 1st SVD mode accounts for a significant 77.1% of tropical Pacific SST variance during the following winter. Consistently, the Z20 expansion coefficients are highly correlated with the Niño3.4 SST time series in

December-January (0.76 correlation, see Table 1), and with the C index defined by Takahashi et al. (2011) to describe the regime of cold and weak-to-moderate ENSO events (0.77 correlation, see Table 1). Note, however, that its performance is only modest for the E index of Takahashi et al. (2011), which accounts for the extreme warm events in the eastern Pacific. In Fig. 1c, the correspondence between the standardized Z20 EC and Niño3.4 SST time series illustrates how well this Z20 precursor is able to anticipate many El Niño (4/8) and La Niña (5/6) events during 1979-2008. This predictor is particularly successful in predicting the transition from El Niño to La Niña phases (e.g. in 1983-84, 1987-88-89, 1998-99), but seems less skillful in capturing the amplitude of some extreme events, such as the 1982-83 El Niño, and also those occurring since the early 2000s (see Fig. 1c; McPhaden, 2012).

The SVD analysis between the USTR precursor over the [110°E-70°W; 10°S-10°N] domain in FMA and ENSO during the 1979-2011 period illustrates that westerly wind anomalies in the western Pacific during late boreal winter are associated with a typical El Niño peak phase during the following winter (Kug et al., 2005), similar to the SST pattern in Fig. 1b (not shown). Results (in Table 1) suggest that this precursor is also an efficient predictor for the ordinary cold and moderately warm ENSO events. Indeed, the corresponding 1st SVD mode accounts for a significant 78.4% of winter SST variance, and the highest correlation is once again obtained with the Niño3.4 and C indices (0.74 and 0.62 correlation, respectively).

4.2 New combined extratropical SST predictor

We now examine the predicting potential for ENSO which stems from extratropical SSTs. Results from the SVD between the new SST predictor and ENSO during the 1979-2011 period are shown in Fig. 2 and Table 1. The precursor fields (Fig. 2a) are characterized by anomalous SST dipoles in the North Pacific, South AO and IO during late boreal winter, consistent with patterns described by Vimont et al

(2003), Wang et al (2012) and Terray (2011). These extratropical features are associated with a typical El Niño peak phase during the following winter (Fig. 2b), similar although slightly warmer than the SST pattern in Fig. 1b, and with maximum SST anomalies reaching further east in the Pacific.

In terms of statistics, the results are also very promising for ENSO predictability. Although this 1st SVD mode explains one of the least variances during JFM in the precursor region (13.1%), it manages to describe the largest portion of winter SST variability in the tropical Pacific (79.6%) and reaches a maximum of 0.80 correlation with the Niño3.4 SST timeseries in winter (Table 1). This new SST predictor is able to fit *both* the timing and amplitude of ENSO events, and this not only in the transition from El Niño to La Niña events, but also when an El Niño develops from a previous neutral or La Niña state in the tropical Pacific (see Fig. 2c, e.g. in 1982-83, 1995-96). Although its performance seems also degraded since the early 2000s, this SST predictor is also successful in capturing the amplitude of *extreme* El Niño events (both in 1982-83 and 1997-98). These results are consistent with the high correlation value obtained with the E index (0.48 in Table 1). However, the observed correlations between the different predictors and the Niño3.4 SST timeseries (or the E and C indices) given in Table 1 are not significantly different from each other according to a statistical test based on the Fisher's Z transformation, due to the shortness of the observed record (Fisher, 1970, p. 199).

4.3. Robustness and predictive relationships

In view of the short observational record, we performed similar SVD analyses with the simulated fields from the SINTEX-F2 CGCM (Table 1; Figs. 2d-f). Overall, results are quite consistent with observations, as this model exhibits a realistic simulation of the relationships of ENSO with both the Z20 and USTR precursors, and the new SST precursor. In Fig. 2d, the precursor SST pattern displays similar dipole

structures as in Fig. 2a (although the simulated SST signal is weaker in the South AO and shifted westwards in the North Pacific), and is also associated with an El Niño peak phase during the following winter, with warm SST anomalies mostly confined to the equatorial central Pacific compared to observations (Fig. 2e). The statistics for the CGCM also show higher correlation values for the new combined SST precursor compared to the Z20 and USTR predictors, although they miss the observed relationship between extratropical SSTs and the E index (see Table 1). Moreover, the correlation of the Niño3.4 SST timeseries with the SST precursor is now significantly higher from those derived from the Z20 and USTR precursors at a significance level of 0.05, thanks to the length of the simulation (Fisher, 1970).

By definition, the high values of the statistics in Table 1 may also partly result from the optimization problem solved by the SVD. In order to assess reliably the predictive potential of the new SST precursor, we also performed a cross-validation experiment of our SVD models. In this experiment, we treated the three precursors in the same objective manner, and re-computed each SVD analysis based successively on all years within the 1979-2008 time span, except one ‘forecast’ year. We then estimated the values of each precursor’s EC time series, by projecting the precursor field observed before the ‘forecast’ year onto the 1st SVD mode computed without this year in the cross-validation procedure. The correlation between the cross-validated SVD modes and Niño3.4 SST shows once again a high correlation for the SST precursor (0.75) compared to the Z20 and USTR precursors (0.67 and 0.65 correlation respectively), although these bootstrapped correlations are again not significantly different at a significance level of 0.05 due to the shortness of the observed record. Similar results are obtained for the E index, while all the precursors have about the same skill for the C index.

In order to provide another test of the usefulness of extratropical SSTs for the prediction of ENSO, Fig A (in auxiliary material) presents the 1st and 2nd EOF modes from the same domain used in the SVD, in both observations and the CGCM. Since results are globally similar in observations and the model (see Fig. A), we will restrict our discussion to observations. Overall, these two EOFs provide some additional insight into the *nature* of the predictability offered by these extratropical SST regions during the 1979-2011 period. Indeed, although both EOF modes seem useful for ENSO prediction (0.27 and 0.59 correlation with Niño3.4 SST during the next winter, see Table A), the predictability offered by the 1st EOF mode is mostly linked to the biennial component of ENSO itself (-0.85 and 0.60 correlations with the concurrent Niño3.4 SST and Z20 EC time series, respectively), whereas the 2nd EOF mode captures a more *intrinsic* extratropical source of predictability, which is independent from the previous ENSO state (0.03 correlation with the concurrent Niño3.4 SST) and moderately linked to the Z20 EC time series (0.5 correlation). Surprisingly, this 2nd EOF has a higher correlation with the winter Niño3.4 SST time series than the 1st EOF, and is also a significant precursor of the E and C indices, as the 1st SVD mode (Table A). Interestingly, the spatial correlations between these first two EOF modes (Fig. Aa and b) and the 1st SST SVD mode (in Fig. 2a) are 0.35 and 0.80, respectively. Consistently, the 1st SVD mode is more correlated with the 2nd EOF time series (0.82) than with the 1st EOF (0.46). Thus, the source of ENSO predictability offered by the 1st SVD mode “combines” both the effects of the ENSO cycle itself and the extratropics, but seems to mainly stem from extratropical variability.

Finally, we developed various regression models for forecasting winter Niño3.4 SST anomalies, using the USTR, Z20 and SST predictors and tested the accuracy of these models with a cross-validation procedure (Clarke and Van Gorder, 2003). In

these cross-validation experiments, we selected the EOF modes for each precutory field which offered the best prediction for the following ENSO: the 1st and 2nd EOF modes for extratropical SSTs (Fig. Aa-b), the 1st EOF mode for tropical Pacific wind anomalies and 2nd EOF mode for Z20 anomalies (same mode as shown in Meinen and McPhaden, 2000). To assess the forecast potential of each model, we then compared the observed Niño3.4 SST with the values calculated from regression equations based successively on all years within the common 1979-2008 time span, except the forecast year. The correlation coefficient between the observed and forecast Niño3.4 SST and the Root-Mean-Square-Error (RMSE) for each model are shown in Table 2, and overall support the proposition that extratropical SSTs are a useful parameter in ENSO forecasts. Indeed, the regression model with the SST predictor as sole input achieves a higher correlation score and lower RMSE than the model which uses both USTR and Z20 predictors (0.64 compared to 0.61 correlation, 0.75 compared to 0.78 RMSE). When combining these 3 predictors, the performance of the multiple regression model is improved (with 0.71 correlation and 0.69 RMSE). Finally, when removing the USTR, the performance of the model is not degraded (see Table 2). This regression exercise thus illustrates how the inclusion of extratropical SSTs may improve the statistical models currently used to predict ENSO.

3.4 Atmospheric variability associated with the new SST predictor

In order to explore the predicting paths of the SST predictor, we have regressed the SST and atmospheric anomalies from the previous summer to the following boreal winter onto the first two leading EOFs of extratropical SSTs in observations. As expected, the regression of SST, SLP and 850 hPa wind anomalies onto the 1st EOF mode depicts the rapid transition from La Niña to El Niño (or El Niño to La Niña since the analysis is linear) and the related changes in teleconnection patterns

elsewhere (see Fig. B in auxiliary material). Note, however, that the ENSO signal predicted by this mode is of limited amplitude and only marginally significant.

Fig. 3 displays the maps of SST, SLP and 850 hPa wind anomalies regressed onto the 2nd EOF of JFM extratropical SSTs. During the previous JAS season, no coherent SST or SLP patterns are found in the tropics, nor in the extratropics, except in the South Pacific (Fig. 3a and g). From boreal fall to winter, a significant anomalous SLP dipole emerges in the central North Pacific (Fig. 3b) consistent with the “Seasonal Footprinting Mechanism” of Vimont et al. (2003), followed one season later by large anticyclonic anomalies over the South AO and IO, which reflect the occurrence of blocking events during late boreal winter or early boreal spring in the Southern Hemisphere (Fig. 3c). These atmospheric phenomena lead to the emergence of a boomerang warm SST structure (Fig. 3i-j) in the North Pacific (Vimont et al. 2003) and to subtropical SST dipoles in the South AO and IO (Hermes and Reason, 2005). Figs. 3c and i also suggest that the extratropical cold SST anomalies over the eastern IO and western North Pacific promote persistent westerly wind anomalies over the western equatorial Pacific from boreal winter to spring (Xu and Chan, 2001; Wang et al., 2012). This westerly equatorial wind signal is a possible trigger of El Niño onset, as it can induce eastward-propagating downwelling Kelvin waves along the thermocline, leading to an El Niño warming several months later.

However, there are also suggestions of additional predicting paths, not restricted to surface wind variability over the western equatorial Pacific. Indeed, from the JFM/AMJ season (Fig. 3c), a significant pattern emerges over the South Pacific, characterized by a weakening of the southeast trade winds and the development of an expanded trough. This slowdown of the Walker circulation induced by South Pacific atmospheric variability may be involved in El Niño onset (Van Loon, 1984; Clement

et al., 2011). South AO and IO anomalies could also be involved in this by remotely impacting the southwest Pacific through a modulation of the regional Hadley cell in boreal spring (Terray and Dominiak, 2005; Terray, 2011). By exciting Rossby waves, these modulations can induce a displacement of the westerly jet stream and low-level circulation in the South Pacific (Trenberth et al., 1998) and lead to the development of the southern branch of the traditional ‘horseshoe’ El Niño pattern (Fig. 3k-l).

5. Conclusions and future work

In this work, we demonstrate that, in addition to well-recognized precursors of El Niño onsets, extratropical SSTs in the North Pacific, South AO and IO during late boreal winter may provide some important information for the forecast of ENSO events. This new ‘combined’ SST precursor is most significantly correlated with the Niño3.4 SST time series during the post-1979 period, and offers some potential *added value* in the prediction of the *amplitude* of these ENSO events. We have further tested the performance of these predictors through various cross-validation experiments and shown that these promising predictive relationships are also quite well reproduced in a comprehensive CGCM.

Our regression analyses confirm that extratropical SST variability may be impacting ENSO through a modulation of wind variability in the western equatorial Pacific during boreal spring (Vimont et al., 2003; Terray, 2011; Wang et al., 2012), but not only. Our results also suggest that the extratropical atmospheric variability may play a significant role in ENSO development by modulating the southeast trades in the South Pacific during boreal spring, particularly for the extraordinary warm events, consistent with several recent studies (Chang et al., 2007; Clement et al., 2011).

Given the suspected importance of this extratropical forcing on ENSO, it now seems essential to gain a better understanding of the physical processes operating between

extratropical and tropical latitudes before the onset of ENSO events, as well as the relative contribution of each hemisphere in this prediction. Do each of these extratropical sectors play independently? Or does this important source of predictability for ENSO result from an interaction between the different basins? Another important question raised by this work is whether the observed relationship between extreme warm events and extratropical SSTs during recent decades is a future characteristic of a global warming climate.

Acknowledgments: This work has been financially supported by the EMBRACE EU project (N°228320). Simulations were performed on the IDRIS super computer.

References

- Bretherton, C., C. Smith, and J. Wallace (1992), An intercomparison of methods for finding coupled patterns in climate data, *J. Clim.*, 5, 541–560.
- Carton, J. A. and B. S. Giese (2008), A Reanalysis of Ocean Climate Using Simple Ocean Data Assimilation (SODA), *Mon. Weather Rev.*, 136, 2999–3017.
- Chang, P. and co-authors (2007), Pacific meridional mode and El Niño–Southern Oscillation. *Geophys. Res. Lett.*, 34, L16608, doi:10.1029/2007GL030302.
- Clarke, A. J., and S. Van Gorder (2003), Improving El Niño prediction using a space-time integration of Indo-Pacific winds and equatorial Pacific upper ocean heat content, *Geophys. Res. Lett.*, 30, 1399.
- Clement, A., P. DiNezio, and C. Deser (2011), Rethinking the ocean’s role in the Southern Oscillation, *J. Clim.*, 24, 4056–4072.
- Cleveland, R. B. and co-authors (1990) A Seasonal-Trend Decomposition Procedure Based on Loess (with discussion). *J Official Statistics*, 6:3–73.
- Dee and co-authors (2011) The ERA-Interim reanalysis: configuration and performance of the data assimilation system. *Quart. J. R. Met. Soc.*, 137, 553–597.

324 Dommenget, D., V. Semenov, and M. Latif (2006), Impacts of the tropical Indian and
 325 Atlantic oceans on ENSO, *Geophys. Res. Lett*, *33*, L11, 701.
 326 Ebisuzaki, W. (1997), A method to estimate the statistical significance of a correlation
 327 when the data are serially correlated, *J. Clim.*, *10*, 2147-2153.
 328 Fisher, R. A. (1970), Statistical Methods for Research Workers, Fourteenth Edition,
 329 Davien, CT: Hafner Publishing Company.
 330 Frauen, C., and D. Dommenget (2012), Influences of the tropical Indian and Atlantic
 331 Oceans on the predictability of ENSO, *Geophys. Res. Lett*, *39*, L02706.
 332 Hermes, J. C., and C. J. C. Reason (2005), Ocean model diagnosis of interannual
 333 coevolving SST variability in the South Indian and South Atlantic Oceans, *J. Clim.*,
 334 *18*, 2864-2882.
 335 Izumo, T. and co-authors (2010), Influence of the state of the Indian Ocean Dipole on
 336 the following years El Niño, *Nature Geoscience*, *3*, 168–172.
 337 Kug, J. S., S. I. An, F. F. Jin, and I. S. Kang (2005), Preconditions for El Niño and La
 338 Niña onsets and their relation to the Indian ocean, *Geophys. Res. Lett.*, *32*, L05, 706.
 339 Masson, S. and co-authors (2012), Impact of intra-daily SST variability on ENSO
 340 characteristics in a coupled model, *Clim. Dyn.*, *39*, 729-754.
 341 McPhaden, M. J. (2003), Tropical Pacific Ocean heat content variations and ENSO
 342 persistence barriers, *Geophys. Res. Lett*, *30*, 1480.
 343 McPhaden, M. J. (2012), A 21st Century Shift in the Relationship between ENSO SST
 344 and Warm Water Volume Anomalies. *Geophys. Res. Lett.*, *39*, L09706.
 345 Meinen, C. S., and M. J. McPhaden (2000), Observations of Warm Water Volume
 346 changes in the equatorial pacific and their relationship to El Niño and La Niña, *J.*
 347 *Clim.*, *13*, 3551–3559.

348 Rayner, N. A., and co-authors (2003), Global analyses of sea surface temperature, sea
 349 ice, and night marine air temperature since the late nineteenth century, *J. Geophys.*
 350 *Res.*, *108*(D14), 4407, doi:10.1029/2002JD002670.
 351 Rodriguez-Fonseca, B., and co-authors (2009), Are Atlantic Niños enhancing Pacific
 352 ENSO events in recent decades, *Geophys. Res. Lett.*, *36*, L20, 705.
 353 Takahashi, K., A. Montecinos, K. Goubanova, and B. Dewitte (2011), ENSO regimes:
 354 Reinterpreting the canonical and Modoki El Niño. *Geophys. Res. Lett.*, *38*, L10704.
 355 Terray, P., and S. Dominiak (2005), Indian Ocean Sea Surface Temperature and El
 356 Niño-Southern Oscillation: a new perspective, *J. Clim.*, *18*, 1351–1368.
 357 Terray, P. (2011), Southern hemisphere extra-tropical forcing: a new paradigm for El
 358 Niño-Southern Oscillation, *Clim. Dyn.*, *36*, 2171–2199.
 359 Trenberth, K.E., G. W. Branstator, D. Karoly, A. Kumar, N.-C. Lau, C. Ropelewski
 360 (1998), Progress during TOGA in understanding and modeling global teleconnections
 361 associated with tropical sea surface temperatures, *J. Geophys. Res.*, *103*, 14291–14324.
 362 Van Loon, H. (1984) The Southern Oscillation. Part III: Associations with the trades
 363 and with the trough in the westerlies of the South Pacific Ocean, *Mon. Wea Rev.*, *112*.
 364 Vimont, D. J., D. S. Battisti, and A. C. Hirst (2003), The seasonal footprinting
 365 mechanism in the CSIRO general circulation models, *J. Clim.*, *16*, 2653–2667.
 366 Wang, S.-Y., M. L’Heureux, H.-H. Chia (2012) ENSO prediction one year in advance
 367 using Western North Pacific sea surface temperatures, *Geophys. Res. Lett.*, *39*, L05702.
 368 Webster, P. J., and S. Yang (1992), Monsoon and ENSO: Selectively interactive
 369 systems, *Q. J. R. Meteorol. Soc.*, *118*, 877–926.
 370 Xu J. and J. C. L. Chan (2001), The Role of the Asian-Australian Monsoon System in
 371 the Onset Time of El Niño Events, *J. Clim.*, *14*, 418–433.

372

Table 1: Statistics associated with the 1st SVD modes between Z20, USTR or the new ‘combined’ SST precursor during late boreal winter and ENSO SST anomalies in the tropical Pacific during the following winter. The last 3 columns give the correlation between each SVD mode and various ENSO indices during the next December-January season: the Niño3.4 SST index, the C and E indices used in Takahashi et al. (2011). Results are given for observations (in red) and for the model (in blue). The correlation coefficients exceeding the 10%, 5% and 1% confidence levels according to the phase-scrambling bootstrap test of Ebisuzaki (1997) are followed by one asterisk (*), two asterisks (**), and three asterisks (***), respectively.

<i>SVD results</i> <i>Precursor</i>	SCF (%)		r		Precursor var (%)		ENSO var (%)		Cor Niño3.4		Cor C index		Cor E index	
Z20	84.5	87	0.71	0.56	12.9	24.3	77.1	63.3	0.76***	0.55***	0.77***	0.52***	0.35	0.22**
Ustr	89.3	84.9	0.64	0.53	21.1	21.5	78.4	67.1	0.74***	0.54***	0.62***	0.54***	0.32	0.21*
‘combined’ SST	90.8	83.1	0.78	0.71	13.1	8.1	79.6	69	0.80***	0.71***	0.67***	0.70***	0.48**	0.11

* P<0.1, **P<0.05, ***P<0.01

Table 2: Forecast skill of simple linear regression models using two (A and B), three (D) or four (C) predictors in JFM as inputs for the prediction of the Niño3.4 time series during the following December-January. As input for each model, we select the EOF modes associated with the Z20, USTR and SST precursors, which offer the best prediction for the following ENSO. The forecast skill of each model is assessed by the cross-validated correlation and root-mean-square-error (RMSE) calculated between the observed and forecast Niño3.4 time series, without involving the forecast year.

Regression models	<i>Selected EOF mode</i>	<i>Correlation</i>	<i>RMSE</i>
A) with SST predictors	SST (eof m1) + SST (eof m2)	0.64	0.75
B) with Z20 and USTR predictors	Z20 (eof m2) + USTR (eof m1)	0.61	0.78
C) with SST, Z20 and USTR predictors	SST (eof m1) + SST (eof m2) + Z20 (eof m2) + USTR (eof m1)	0.71	0.69
D) with SST and Z20 predictors	SST (eof m1) + SST (eof m2) + Z20 (eof m2)	0.72	0.68

1
2 **Extratropical forcing of ENSO**
3
4

5 Ghyslaine Boschat¹, Pascal Terray², Sébastien Masson³
6

7 *LOCEAN/IPSL, CNRS/IRD/UPMC/MNHN, Paris, France*
8
9
10
11
12
13

14 To be submitted to *Geophysical Research Letters*
15

16 December 2012

17 February 2013
18
19

¹ Corresponding author: Ghyslaine Boschat, LOCEAN-IPSL,
Université Pierre et Marie Curie, BP100 – 4 place Jussieu, 75252 Paris cedex 05, France.
Tel : +33 1 44 27 23 29
E-mail : gbolod@locean-ipsl.upmc.fr

² Pascal TERRAY, LOCEAN-IPSL, UMR 7617 CNRS/IRD/UPMC/MNHN
Université Pierre et Marie Curie, BP 100 - 4 Place Jussieu 75252 Paris cedex 05 France
Tel : +33 1 44 27 70 78
E-mail : pascal.terray@locean-ipsl.upmc.fr

³ Sébastien MASSON, LOCEAN-IPSL,
Université Pierre et Marie Curie, BP100 – 4 place Jussieu, 75252 Paris cedex 05, France.
Tel : +33 1 44 27 27 48
E-mail : sebastien.masson@locean-ipsl.upmc.fr

1. Abstract

We present evidence that Sea Surface Temperatures (SSTs) in the North Pacific, South Atlantic and Indian Oceans (AO and IO, respectively) during late boreal winter, offer another important source of predictability for El Niño Southern Oscillation (ENSO). This new SST predictor may provide accurate prediction of the *amplitude* of ENSO events before their onset, for both El Niño and La Niña events, ~~and especially for the extreme warm events~~, which occurred during recent decades.

2. Introduction

According to many studies, the crucial set of information for ENSO forecasts lies in the spatial variation of the thermocline depth or heat content (Meinen and McPhaden, 2000; McPhaden 2003) and the low-frequency wind variability in the tropical Indo-Pacific region (Clarke and Van Gorder, 2003). An influence from high-frequency wind variability in the western Pacific region has also been suggested, but so far the most robust leading relationship has been observed with the Madden Julian Oscillation activity in late boreal spring or early summer, therefore after the ENSO onset period (Hendon et al., 2007).

Nevertheless, there has been growing evidence in the literature, that other tropical and extratropical regions may also be playing an important role for ENSO. First, a number of studies suggested a close link with SST anomalies in the tropical IO or AO, which may induce modulations of the Walker circulations (Kug et al., 2005; Dommenget et al., 2006; ~~Jansen et al., 2009~~; Rodriguez-Fonseca et al., 2009; Izumo et al., 2010; Frauen and Dommenget, 2012). Recently, there has also been a rising interest in the predictability offered by *extratropical* climate modes of variability. Vimont et al. (2003) and Wang et al. (2012) have implied a connection between the

Formatted: Indent: First line: 0.2"

mid-latitude and tropical Pacific, whereby the winter atmospheric variability in the North Pacific impacts subtropical SST variability and western Pacific equatorial wind anomalies, which may be responsible for exciting subsequent El Niño events. Several recent studies also emphasized the role of mid-latitude coupled variability in the South AO and IO during late boreal winter (Terray and Dominiak, 2005; Terray, 2011).

However, several open questions remain regarding the *pertinence* or added value of these new ‘extratropical’ precursors for the forecast of ENSO, compared to the conventional Pacific wind or heat content predictors, or the other tropical SST predictors. In this study, we combine the newly proposed sources of ENSO predictability in the North Pacific, South AO and IO, and evaluate the potential efficiency of this new SST predictor in predicting ENSO onset and amplitude across the “spring predictability barrier” (Webster and Yang, 1992). We present evidence, through statistical analyses of observations and a coupled ocean-atmosphere model simulation, that this new SST precursor may offer an important source of predictability for ENSO, ~~by adding pertinent information regarding the amplitude of events, especially for the extreme warm events (Takahashi et al., 2011).~~

3. Data and Methods

We compare three precursors of ENSO in late boreal winter: the upper-ocean heat content (Z20 precursor) and low-frequency zonal wind stress variability (USTR precursor) in the tropical Pacific, and SST variability in the North Pacific, South AO and IO (new SST precursor). We focus our analysis on the recent period after 1979, since records of tropical Pacific heat content and SST in the South AO and IO are either sparse or inexistent before this date.

The depth of the 20°C isotherm (Z20) is used as a proxy of the thermocline depth or heat content in the tropical Pacific Ocean, and is extracted from the Simple Ocean Data Assimilation (SODA) reanalysis (Carton and Giese, 2008; SODA version 2.2.4), available until 2008. We examine atmospheric fields (~~zonal wind stress (USTR), sea level pressure (SLP), and 850hPa winds~~) from the ERA-Interim reanalysis (Dee et al., 2011) and SST fields from the Hadley Centre Global Sea Ice and Sea Surface Temperature (HadISST1.1) dataset (Rayner et al., 2003), both available until 2011. For each field, monthly anomalies are calculated by applying the Seasonal-Trend decomposition procedure based on Loess (Cleveland et al., 1990), which filters out any long-term trends and annual cycle in the initial data.

Our goal is to predict the ENSO peak phase, which is defined by SST anomalies averaged from October to the following February (ONDJF) over the *entire* equatorial Pacific. The precursors are taken either from January to March (JFM) or February to April (FMA), 9 or 10 months prior to this typical ENSO peak phase. Sensitivity analyses have been performed with the precursors taken successively in JFM, FMA or from March to May (MAM), and for each case, we have chosen the season which offers the best skill for the following ENSO.

In order to compare the Z20, USTR and new SST precursors, we use the Singular Value Decomposition (SVD) method (Bretherton et al., 1992), which we apply separately between each precursor field during its peaking season and the following tropical Pacific SST field during boreal winter. Results are shown for the 1st SVD mode associated with each precursor in terms of the corresponding Expansion Coefficient (EC) time series, the ‘homogeneous’ map for the precursor (i.e regression map between the precursor field and its corresponding EC time series) and ‘heterogeneous’ map for the predicted ENSO field (i.e regression map between the

tropical Pacific SST and the EC time series of the precursor field, indicating how well the grid point anomalies of the ENSO field can be predicted from the precursor's EC time series). The statistics provided by the SVD are also efficient tools for quantifying the relevance of each ENSO precursor. The Squared Covariance Fraction (SCF) measures the relative importance of each SVD mode in reconstructing the covariance matrix between the precursor field and tropical Pacific SSTs. The correlation coefficient (r) between the EC time series of the two fields indicate how strongly related the coupled patterns are. Finally, we computed how much of Pacific SST variance each SVD mode explains, and the correlations between the SVD modes and the Niño3.4 SST time series during the following winter.

To test the robustness of our results, we also performed similar SVD analyses on a 110-year control simulation of the SINTEX-F2 global coupled ocean-atmosphere general (CGCM) model, since it exhibits a realistic ENSO (Masson et al., 2012).

4. Analysis and Results

4.1 Heat content and zonal wind predictors

We here examine the conventional Z20 and USTR predictors and assess their relationships with the following ENSO event, within our SVD framework (Fig. 1 and Table 1). During the 1979-2008 period, the 1st SVD mode between the Z20 precursor and ENSO is consistent with the predicting potential of heat content in the context of ENSO forecasting (McPhaden, 2003). Indeed, the Z20 pattern in Fig. 1 is marked by positive Z20 anomalies in the west-central tropical Pacific in spring and appears as a mixture of the two leading Empirical Orthogonal Functions (EOFs) of Pacific Z20 variability (see Meinen and McPhaden, 2000); while the corresponding SST pattern (Fig. 1b) illustrates a typical El Niño peak phase during the following winter (consistent with figure 5 in McPhaden, 2003). This SST pattern also suggests that the performance of the Z20 precursor is degraded in the far eastern equatorial Pacific.

The statistics of this 1st SVD mode (shown in Table 1) confirm that Z20 anomalies during late boreal winter are strongly correlated with SST anomalies in the tropical Pacific ($r=0.71$), and that this 1st SVD mode accounts for a significant 77.1% of tropical Pacific SST variance during the following winter. Consistently, the Z20 expansion coefficients are highly correlated with the Niño3.4 SST time series in December-January (0.76 correlation, see Table 1), and with the C index defined by Takahashi et al. (2011) to describe the regime of cold and weak-to-moderate ENSO events (0.77 correlation, see Table 1). Note, however, that its performance is only modest for the E index of Takahashi et al. (2011), which accounts for the extreme warm events in the eastern Pacific ~~(e.g. the 1982-83 El Niño event)~~. In Fig. 1c, the correspondence between the standardized Z20 EC and Niño3.4 SST time series illustrates how well this Z20 precursor is able to anticipate many El Niño ~~(4-out-of-8)~~ and La Niña ~~(5-out-of-6)~~ events during 1979-2008. This predictor is particularly successful in predicting the transition from El Niño to La Niña phases (e.g. in 1983-84, 1987-88-89, 1998-99), but seems less skillful in capturing the amplitude of some extreme events, such as the 1982-83 El Niño, and also those occurring since the early 2000s (see Fig. 1c ~~and~~ McPhaden, 2012).

The SVD analysis between the USTR precursor over the [110°E-70°W; 10°S-10°N] domain in FMA and ENSO during the 1979-2011 period illustrates that westerly wind anomalies in the western Pacific during late boreal winter are associated with a typical El Niño peak phase during the following winter (Kug et al., 2005), similar to the SST pattern in Fig. 1b (not shown). Results (in Table 1) suggest that this precursor is also an efficient predictor for the ordinary cold and moderately warm ENSO events. Indeed, the corresponding 1st SVD mode accounts for a

significant 78.4% of winter SST variance, and the highest correlation is once again obtained with the Niño3.4 and C indices (0.74 and 0.62 correlation, respectively).

4.2 New combined extratropical SST predictor

We now examine the predicting potential for ENSO which stems from extratropical SSTs. Results from the SVD between the new SST predictor and ENSO during the 1979-2011 period are shown in Fig. 2 and Table 1. The precursor fields (Fig. 2a) are characterized by anomalous SST dipoles in the North Pacific, South AO and IO during late boreal winter, consistent with patterns described by Vimont et al (2003), Wang et al (2012) and Terray (2011). These extratropical features are associated with a typical El Niño peak phase during the following winter (Fig. 2b), similar although slightly warmer than the SST pattern in Fig. 1b, and with maximum SST anomalies reaching further east in the Pacific.

In terms of statistics, the results are also very promising for ENSO predictability. Although this 1st SVD mode explains one of the least variances during JFM in the precursor region (13.1%), it manages to describe the largest portion of winter SST variability in the tropical Pacific (79.6%) and reaches a maximum of 0.80 correlation with the Niño3.4 SST timeseries in winter (Table 1). ~~Compared to the Z20 predictor,~~ ~~this~~ This new SST predictor is able to fit both the timing and amplitude of ENSO events, and this not only in the transition from El Niño to La Niña events, but also when an El Niño develops from a previous neutral or La Niña state in the tropical Pacific (see Fig. 2c, e.g. in 1982-83, 1995-96). Although its performance seems also degraded since the early 2000s, this SST predictor is ~~particularly~~ also successful in capturing the amplitude of *extreme* El Niño events (both in 1982-83 and 1997-98). These results are consistent with the ~~higher and significant~~ correlation value obtained with the E index (0.48 in Table 1), ~~and thus reflect the potential added value of extratropical SSTs for the predictability of extreme warm ENSO regimes (Takahashi~~

et al., 2014). However, the observed correlations between the different predictors and the Niño3.4 SST timeseries (or the E and C indices) given in Table 1 are not significantly different from each other according to a statistical test based on the Fisher's Z transformation, due to the shortness of the observed record (Fisher, 1970, p. 199).

4.3. Robustness and predictive relationships

In view of the short observational record, we performed similar SVD analyses with the simulated fields from the SINTEX-F2 CGCM (Table 1; Figs. 2d-f). Overall, results are quite consistent with observations, as this model exhibits a realistic simulation of the relationships of ENSO with both the Z20 and USTR precursors, and the new SST precursor. In Fig. 2d, the precursor SST pattern displays similar dipole structures as in Fig. 2a (although the simulated SST signal is weaker in the South AO and shifted westwards in the North Pacific), and is also associated with an El Niño peak phase during the following winter, with warm SST anomalies mostly confined to the equatorial central Pacific compared to observations (Fig. 2e). The statistics for the CGCM also show higher correlation values for the new combined SST precursor compared to the Z20 and USTR predictors, although they miss the observed relationship between extratropical SSTs and the E index (see Table 1). Moreover, the correlation of the Niño3.4 SST timeseries with the SST precursor is now significantly higher from those derived from the Z20 and USTR precursors at a significance level of 0.05, thanks to the length of the simulation (Fisher, 1970).

By definition, the high values of the statistics in Table 1 may also partly result from the optimization problem solved by the SVD. In order to assess reliably the predictive potential of the new SST precursor, we also performed a cross-validation experiment of our SVD models. In this experiment, we treated the three precursors in the same objective manner, and re-computed each SVD analysis based successively

on all years within the 1979-2008 time span, except one ‘forecast’ year. We then estimated the values of each precursor’s EC time series, by projecting the precursor field observed before the ‘forecast’ year onto the 1st SVD mode computed without this year in the cross-validation procedure. The correlation between the cross-validated SVD modes and Niño3.4 SST shows once again a higher-high correlation for the SST precursor (0.75) compared to the Z20 and USTR precursors (0.67 and 0.65 correlation respectively), although these bootstrapped correlations are again not significantly different at a significance level of 0.05 due to the shortness of the observed record. Similar results are obtained for the E index ~~(with a higher 0.42 correlation for the SST precursor, compared to 0.26 and 0.32 correlation for the Z20 and USTR precursors, respectively)~~, while all the precursors have about the same skill for the C index ~~(correlation between 0.65 and 0.67 for each precursor).~~

In order to provide another test of the usefulness of extratropical SSTs for the prediction of ENSO, Fig A (in auxiliary material) presents the 1st and 2nd EOF modes from the same domain used in the SVD, in both observations and the CGCM. Since ~~the results of this EOF analysis~~ are globally similar in observations and the model (see Fig. A), we will restrict our discussion to observations. Overall, these two EOFs provide some additional insight into the *nature* of the predictability offered by these extratropical SST regions during the 1979-2011 period. Indeed, although both EOF modes seem useful for ENSO prediction (0.27 and 0.59 correlation with ~~the~~ Niño3.4 SST ~~index~~ during the next winter, see Table A), the predictability offered by the 1st EOF mode is mostly linked to the biennial component of ENSO itself (-0.85 and 0.60 correlations with the concurrent Niño3.4 SST and Z20 EC time series, respectively), whereas the 2nd EOF mode captures a more *intrinsic* extratropical source of predictability, which is independent from the previous ENSO state (0.03 correlation

222 with the concurrent Niño3.4 SST) and moderately linked to the Z20 EC time series
 223 (0.5 correlation). Surprisingly, this 2nd EOF has a higher correlation with the winter
 224 | Niño3.4 SST time series -than the 1st EOF, and is also a significant precursor of the E
 225 and C indices, as the 1st SVD mode (Table A). Interestingly, the spatial correlations
 226 between these first two EOF modes (Fig. Aa and b) and the 1st SST SVD mode (in
 227 Fig. 2a) are 0.35 and 0.80, respectively. Consistently, the 1st SVD mode is more
 228 correlated with the 2nd EOF time series (0.82) than with the 1st EOF (0.46). Thus, the
 229 source of ENSO predictability offered by the 1st SVD mode “combines” both the
 230 effects of the ENSO cycle itself and the extratropics, but seems to mainly stem from
 231 extratropical variability.

232 Finally, we developed various regression models for forecasting winter Niño3.4
 233 SST anomalies, using the USTR, Z20 and SST predictors and tested the accuracy of
 234 these models with a cross-validation procedure (Clarke and Van Gorder, 2003). In
 235 these cross-validation experiments, we selected the EOF modes for each precursory
 236 field which offered the best prediction for the following ENSO: the 1st and 2nd EOF
 237 modes for extratropical SSTs (Fig. Aa-b), the 1st EOF mode for tropical Pacific wind
 238 anomalies and 2nd EOF mode for Z20 anomalies (same mode as shown in Meinen and
 239 McPhaden, 2000). To assess the forecast potential of each model, we then compared
 240 the observed Niño3.4 SST with the values calculated from regression equations based
 241 successively on all years within the common 1979-2008 time span, except the forecast
 242 year. The correlation coefficient between the observed and forecast Niño3.4 SST and
 243 the Root-Mean-Square-Error (RMSE) for each model are shown in Table 2, and
 244 | overall support the proposition that extratropical SSTs ~~may be a crucial~~are a useful
 245 parameter in ENSO forecasts. Indeed, the regression model with the SST predictor as
 246 sole input achieves a higher correlation score and lower RMSE than the model which

uses both USTR and Z20 predictors (0.64 compared to 0.61 correlation, 0.75 compared to 0.78 RMSE). When combining these 3 predictors, the performance of the multiple regression model is ~~significantly~~ improved (with 0.71 correlation and 0.69 RMSE). Finally, when removing the USTR, the performance of the model is not degraded (see Table 2). This regression exercise thus illustrates how the inclusion of extratropical SSTs may improve the statistical models currently used to predict ENSO.

3.4 Atmospheric variability associated with the new SST predictor

In order to explore the predicting paths of the SST predictor, we have regressed the SST and atmospheric anomalies from the previous summer to the following boreal winter onto the first two leading EOFs of extratropical SSTs in observations. As expected, the regression of SST, SLP and 850 hPa wind anomalies onto the 1st EOF mode depicts the rapid transition from La Niña to El Niño (or El Niño to La Niña since the analysis is linear) and the related changes in teleconnection patterns elsewhere (see Fig. B in auxiliary material). Note, however, that the ENSO signal predicted by this mode is of limited amplitude and only marginally significant.

Fig. 3 displays the maps of SST, SLP and 850 hPa wind anomalies regressed onto the 2nd EOF of JFM extratropical SSTs. During the previous JAS season, no coherent SST or SLP patterns are found in the tropics, nor in the extratropics, except in the South Pacific (Fig. 3a and g). From boreal fall to winter, a significant anomalous SLP dipole emerges in the central North Pacific (Fig. 3b) consistent with the “Seasonal Footprinting Mechanism” of Vimont et al. (2003), followed one season later by large anticyclonic anomalies over the South AO and IO, which reflect the occurrence of blocking events during late boreal winter or early boreal spring in the Southern Hemisphere (Fig. 3c). These atmospheric phenomena lead to the emergence of a boomerang warm SST structure (Fig. 3i-j) in the North Pacific (Vimont et al. 2003)

and to subtropical SST dipoles in the South AO and IO (Hermes and Reason, 2005). Figs. 3c and i also suggest that the extratropical cold SST anomalies over the eastern IO and western North Pacific promote persistent westerly wind anomalies over the western equatorial Pacific from boreal winter to spring (Xu and Chan, 2001; Wang et al., 2012). This westerly equatorial wind signal is a possible trigger of El Niño onset, as it can induce eastward-propagating downwelling Kelvin waves along the thermocline, leading to an El Niño warming several months later.

However, there are also suggestions of additional predicting paths, not restricted to surface wind variability over the western equatorial Pacific. Indeed, from the JFM/AMJ season (Fig. 3c), a significant pattern emerges over the South Pacific, characterized by a weakening of the southeast trade winds and the development of an expanded trough. This slowdown of the Walker circulation induced by South Pacific atmospheric variability may be involved in El Niño onset (Van Loon, 1984; Clement et al., 2011). South AO and IO anomalies could also be involved in this by remotely impacting the southwest Pacific through a modulation of the regional Hadley cell ~~during-in~~ boreal spring (Terray and Dominiak, 2005; Terray, 2011). By exciting Rossby waves, these modulations can induce a displacement of the westerly jet stream and low-level circulation in the South Pacific (Trenberth et al., 1998) and lead to the development of the southern branch of the traditional ‘horseshoe’ El Niño pattern (Fig. 3k-l).

5. Conclusions and future work

In this work, we demonstrate that, in addition to well-recognized precursors of El Niño onsets, extratropical SSTs in the North Pacific, South AO and IO during late boreal winter may provide some important information for the forecast of ENSO events. This new ‘combined’ SST precursor is most significantly correlated with the

Niño3.4 SST time series during the post-1979 period, and offers some potential *added value* in the prediction of the *amplitude* of these ENSO events. We have further tested the performance of these predictors through various cross-validation experiments and shown that these promising predictive relationships are also quite well reproduced in a comprehensive CGCM.

Our regression analyses confirm that extratropical SST variability may be impacting ENSO through a modulation of wind variability in the western equatorial Pacific during boreal spring (Vimont et al., 2003; Terray, 2011; Wang et al., 2012), but not only. Our results also suggest that the extratropical atmospheric variability may play a significant role in ENSO development by modulating the southeast trades in the South Pacific during boreal spring, particularly for the extraordinary warm events, consistent with several recent studies (Chang et al., 2007; Clement et al., 2011).

Given the suspected importance of this extratropical forcing on ENSO, it now seems essential to gain a better understanding of the physical processes operating between extratropical and tropical latitudes before the onset of ENSO events, as well as the relative contribution of each hemisphere in this prediction. Do each of these extratropical sectors play ~~separately, and~~ independently? Or does this important source of predictability for ENSO result from an interaction between the different basins? Another important question raised by this work is whether the observed relationship between extreme warm events and extratropical SSTs during recent decades is a future characteristic of a global warming climate.

Acknowledgments: This work has been financially supported by the EMBRACE EU project (N°228320). Simulations were performed on the IDRIS super computer.

References

322 Bretherton, C., C. Smith, and J. Wallace (1992), An intercomparison of methods for
 323 finding coupled patterns in climate data, *J. Clim.*, 5, 541–560.

324 Carton, J. A. and B. S. Giese (2008), A Reanalysis of Ocean Climate Using Simple
 325 Ocean Data Assimilation (SODA), *Mon. Weather Rev.*, 136, 2999-3017.

326 Chang, P. and co-authors (2007), Pacific meridional mode and El Niño–Southern
 327 Oscillation. *Geophys. Res. Lett.*, 34, L16608, doi:10.1029/2007GL030302.

328 Clarke, A. J., and S. Van Gorder (2003), Improving El Niño prediction using a space-
 329 time integration of Indo-Pacific winds and equatorial Pacific upper ocean heat
 330 content, *Geophys. Res. Lett.*, 30, 1399.

331 Clement, A., P. DiNezio, and C. Deser (2011), Rethinking the ocean’s role in the
 332 Southern Oscillation, *J. Clim.*, 24, 4056-4072.

333 Cleveland, R. B. and co-authors (1990) A Seasonal-Trend Decomposition Procedure
 334 Based on Loess (with discussion). *J. Official Statistics*, 6:3-73.

335 Dee and co-authors (2011) The ERA-Interim reanalysis: configuration and
 336 performance of the data assimilation system. *Quart. J. R. Met. Soc.*, 137, 553-597.

337 Dommenget, D., V. Semenov, and M. Latif (2006), Impacts of the tropical Indian and
 338 Atlantic oceans on ENSO, *Geophys. Res. Lett.*, 33, L11, 701.

339 Ebisuzaki, W. (1997), A method to estimate the statistical significance of a correlation
 340 when the data are serially correlated, *J. Clim.*, 10, 2147-2153.

341 [Fisher, R. A. \(1970\), Statistical Methods for Research Workers, Fourteenth Edition,](#)
 342 [Davien, CT: Hafner Publishing Company.](#)

343 Frauen, C., and D. Dommenget (2012), Influences of the tropical Indian and Atlantic
 344 Oceans on the predictability of ENSO, *Geophys. Res. Lett.*, 39, L02706.

345 Hermes, J. C., and C. J. C. Reason (2005), Ocean model diagnosis of interannual
 346 coevolving SST variability in the South Indian and South Atlantic Oceans, *J. Clim.*,
 347 *18*, 2864-2882.
 348 Izumo, T. and co-authors (2010), Influence of the state of the Indian Ocean Dipole on
 349 the following years El Niño, *Nature Geoscience*, *3*, 168–172.
 350 ~~Jansen, M. F., D. Dommenget, and N. Keenlyside, Tropical atmosphere-ocean~~
 351 ~~interactions in a conceptual Framework (2009), *J. Clim.*, *22*, 550–567.~~
 352 Kug, J. S., S. I. An, F. F. Jin, and I. S. Kang (2005), Preconditions for El Niño and La
 353 Niña onsets and their relation to the Indian ocean, *Geophys. Res. Lett.*, *32*, L05, 706.
 354 Masson, S. and co-authors (2012), Impact of intra-daily SST variability on ENSO
 355 characteristics in a coupled model, *Clim. Dyn.*, *39*, 729-754.
 356 McPhaden, M. J. (2003), Tropical Pacific Ocean heat content variations and ENSO
 357 persistence barriers, *Geophys. Res. Lett.*, *30*, 1480.
 358 McPhaden, M. J. (2012), A 21st Century Shift in the Relationship between ENSO SST
 359 and Warm Water Volume Anomalies. *Geophys. Res. Lett.*, *39*, L09706.
 360 Meinen, C. S., and M. J. McPhaden (2000), Observations of Warm Water Volume
 361 changes in the equatorial pacific and their relationship to El Niño and La Niña, *J.*
 362 *Clim.*, *13*, 3551–3559.
 363 Rayner, N. A., and co-authors (2003), Global analyses of sea surface temperature, sea
 364 ice, and night marine air temperature since the late nineteenth century, *J. Geophys.*
 365 *Res.*, *108*(D14), 4407, doi:10.1029/2002JD002670.
 366 Rodriguez-Fonseca, B., and co-authors (2009), Are Atlantic Niños enhancing Pacific
 367 ENSO events in recent decades, *Geophys. Res. Lett.*, *36*, L20, 705.
 368 Takahashi, K., A. Montecinos, K. Goubanova, and B. Dewitte (2011), ENSO regimes:
 369 Reinterpreting the canonical and Modoki El Niño. *Geophys. Res. Lett.*, *38*, L10704.

370 Terray, P., and S. Dominiak (2005), Indian Ocean Sea Surface Temperature and El
 371 Niño-Southern Oscillation: a new perspective, *J. Clim.*, *18*, 1351–1368.
 372 Terray, P. (2011), Southern hemisphere extra-tropical forcing: a new paradigm for El
 373 Niño-Southern Oscillation, *Clim. Dyn.*, *36*, 2171–2199.
 374 Trenberth, K.E., G. W. Branstator, D. Karoly, A. Kumar, N.-C. Lau, C. Ropelewski
 375 (1998), Progress during TOGA in understanding and modeling global teleconnections
 376 associated with tropical sea surface temperatures, *J. Geophys. Res.*, *103*, 14291-14324.
 377 Van Loon, H. (1984) The Southern Oscillation. Part III: Associations with the trades
 378 and with the trough in the westerlies of the South Pacific Ocean, *Mon. Wea Rev.*, *112*.
 379 Vimont, D. J., D. S. Battisti, and A. C. Hirst (2003), The seasonal footprinting
 380 mechanism in the CSIRO general circulation models, *J. Clim.*, *16*, 2653–2667.
 381 Wang, S.-Y., M. L’Heureux, H.-H. Chia (2012) ENSO prediction one year in advance
 382 using Western North Pacific sea surface temperatures, *Geophys. Res. Lett.*, *39*, L05702.
 383 Webster, P. J., and S. Yang (1992), Monsoon and ENSO: Selectively interactive
 384 systems, *Q. J. R. Meteorol. Soc.*, *118*, 877–926.
 385 Xu J. and J. C. L. Chan (2001), The Role of the Asian-Australian Monsoon System in
 386 the Onset Time of El Niño Events, *J. Clim.*, *14*, 418-433.
 387

Table 1: Statistics associated with the 1st SVD modes between Z20, USTR or the new ‘combined’ SST precursor during late boreal winter and ENSO SST anomalies in the tropical Pacific during the following winter. The last 3 columns give the correlation between each SVD mode and various ENSO indices during the next December-January season: the Niño3.4 SST index, the C and E indices used in Takahashi et al. (2011). Results are given for observations (in red) and for the model (in blue). The correlation coefficients exceeding the 10%, 5% and 1% confidence levels according to the phase-scrambling bootstrap test of Ebisuzaki (1997) are followed by one asterisk (*), two asterisks (**) and three asterisks (***), respectively.

<i>SVD results</i> <i>Precursor</i>	SCF (%)		r		Precursor var (%)		ENSO var (%)		Cor Niño3.4		Cor C index		Cor E index	
Z20	84.5	87	0.71	0.56	12.9	24.3	77.1	63.3	0.76***	0.55***	0.77***	0.52***	0.35	0.22**
Ustr	89.3	84.9	0.64	0.53	21.1	21.5	78.4	67.1	0.74***	0.54***	0.62***	0.54***	0.32	0.21*
‘combined’ SST	90.8	83.1	0.78	0.71	13.1	8.1	79.6	69	0.80***	0.71***	0.67***	0.70***	0.48**	0.11

* P<0.1, **P<0.05, ***P<0.01

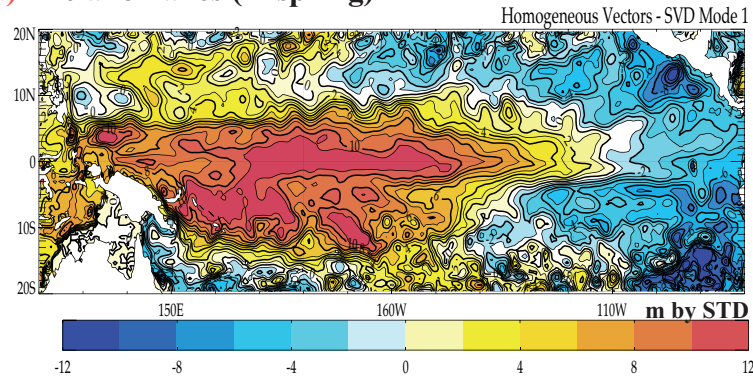
Table 2: Forecast skill of simple linear regression models using two (A and B), three (D) or four (C) predictors in JFM as inputs for the prediction of the Niño3.4 time series during the following December-January. As input for each model, we select the EOF modes associated with the Z20, USTR and SST precursors, which offer the best prediction for the following ENSO. The forecast skill of each model is assessed by the cross-validated correlation and root-mean-square-error (RMSE) calculated between the observed and forecast Niño3.4 time series, without involving the forecast year.

Regression models	<i>Selected EOF mode</i>	<i>Correlation</i>	<i>RMSE</i>
A) with SST predictors	SST (eof m1) + SST (eof m2)	0.64	0.75
B) with Z20 and USTR predictors	Z20 (eof m2) + USTR (eof m1)	0.61	0.78
C) with SST, Z20 and USTR predictors	SST (eof m1) + SST (eof m2) + Z20 (eof m2) + USTR (eof m1)	0.71	0.69
D) with SST and Z20 predictors	SST (eof m1) + SST (eof m2) + Z20 (eof m2)	0.72	0.68

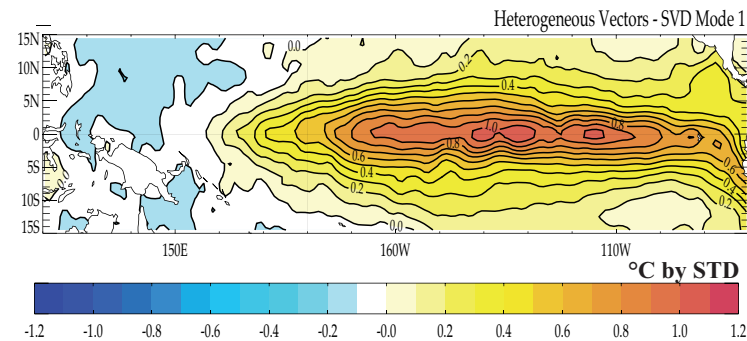
Figure 1 : Observed 1st SVD mode between Z20 precursor over [110°E-70°W; 20°S-20°N] and tropical Pacific SST over [120°E-80°W; 15°S-15°N] during 1979-2008: **(a)** Z20 homogeneous map in JFM, **(b)** Pacific SST heterogeneous map in ONDJF, and **(c)** standardized Z20 EC time series in JFM (black curve) superimposed with the standardized Niño3.4 SST time series in the following December-January season (red curve). The blue (green) crosses indicate the number of predicted El Niño (La Niña) events (e.g. when both time series exceed a 0.75 standard deviation threshold).

SVD (Z20-ENSO) - obs

a) Z20 anomalies (in spring)



b) SST anomalies (in winter)



c) Z20 Expansion Coefficient and Nino3.4 SST timeseries

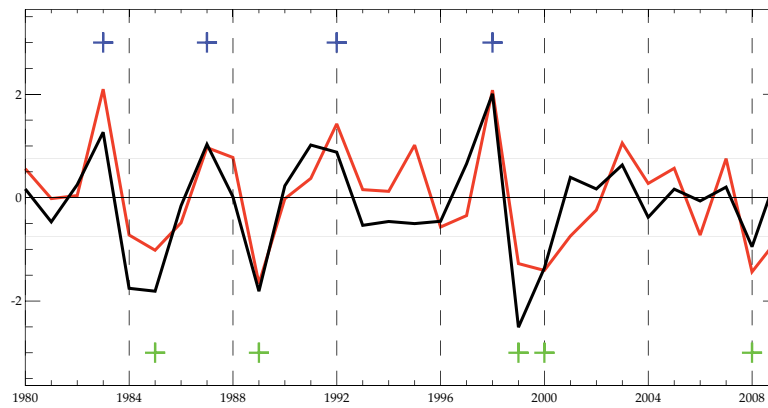


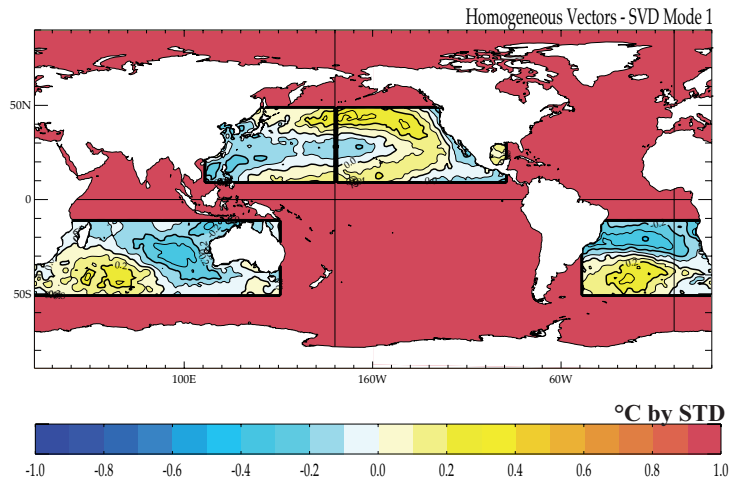
Figure 2 : As in Figure 1, but for the observed 1st SVD mode between the JFM extratropical SST precursor (over the North Pacific [110°E-90°W; 10°N-50°N], South Indian [25°E-150°E; 10°S-50°S] and South Atlantic [50°W-25°E; 10°S-50°S] Oceans) and winter tropical Pacific SST during the 1979-2011 period (**panels a,b,c**) and the SINTEX-F2 simulation (**panels d,e,f**). The SST EC time series manages to predict 12 out of the 20 El Niño events, and 14 out of the 24 La Niña events in this control simulation.

SVD (Combined SST precursor-ENSO)

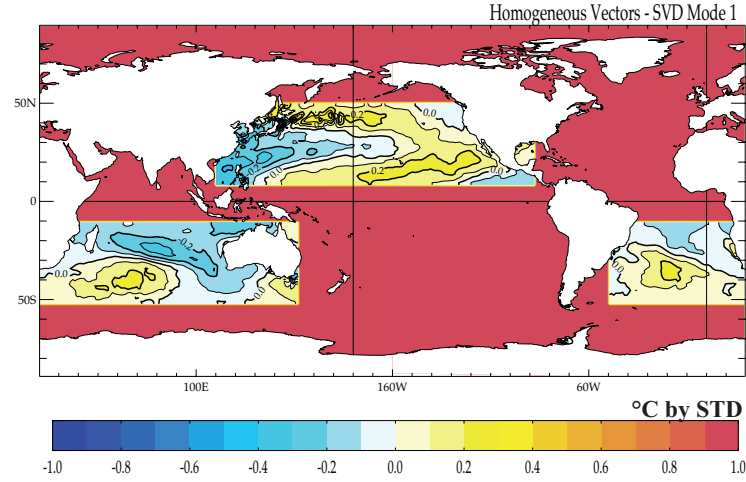
OBSERVATIONS

MODEL

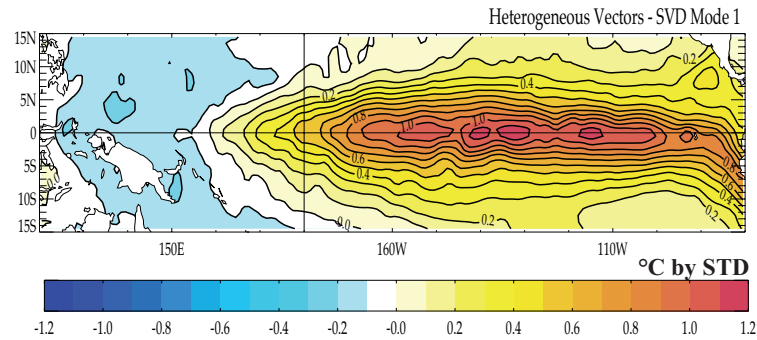
a) SST anomalies (in spring)



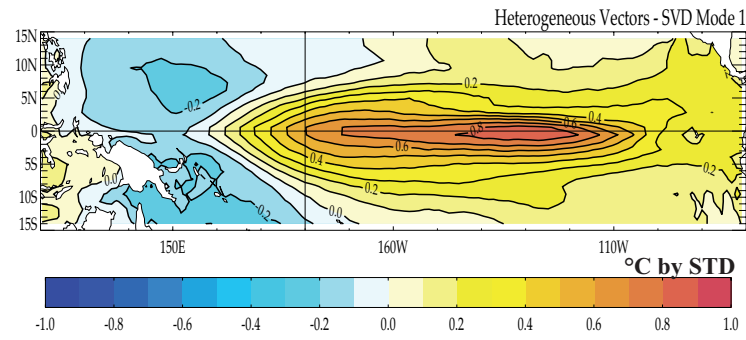
d)



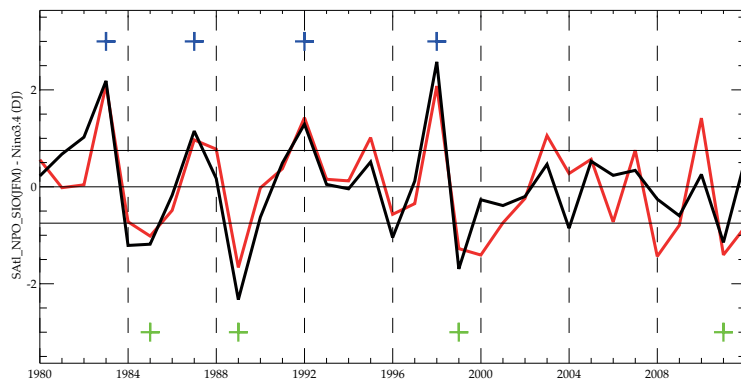
b) SST anomalies (in winter)



e)



c) SST Expansion Coefficient and Nino3.4 SST timeseries



f)

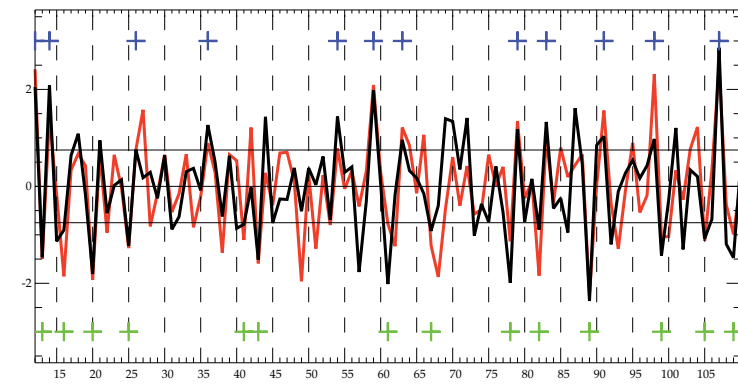


Figure 3 : Sea Level Pressure (SLP, shading) and 850hPa wind (vectors) anomalies (a to f) and SST anomalies (g to l) regressed onto the 2nd EOF time series of extratropical SST in JFM (over the 1979-2011 period). Maps are shown from the previous boreal summer to the following boreal winter. The black contours and the wind vectors denote that the corresponding correlation coefficients are above the 90% confidence level following a phase-scrambling procedure with 999 samples

